

Article

Are the Fenno-Scandinavian Arctic Wetlands a Significant Regional Source of Formic Acid?

Benjamin T. Jones¹, Jennifer Muller¹, Sebastian O'Shea¹, Asan Bacak¹, Grant Allen¹, Martin Gallagher¹, Keith Bower¹, Michael Le Breton¹, Thomas J. Bannan², Stephane Bauguitte³, John Pyle², Dave Lowry⁴, Rebecca Fisher⁴, James France⁴, Euan Nisbet⁴, Dudley Shallcross⁵ and Carl Percival^{1,*†}

¹ School of Earth, Atmospheric and Environmental Sciences, University of Manchester, Oxford Road, Manchester M13 9PL, UK; benjamin.jones-4@hotmail.co.uk (B.T.J.); Jennifer.Mueller@dwd.de (J.M.); sebastian.oshea@manchester.ac.uk (S.O.); asan.bacak@manchester.ac.uk (A.B.); grant.allen@manchester.ac.uk (G.A.); martin.gallagher@manchester.ac.uk (M.G.); k.bower@manchester.ac.uk (K.B.); michael.le.breton@gu.se (M.L.B.)

² National Centre for Atmospheric Science–Climate, Department of Chemistry, University of Cambridge, Cambridge CB2 1EW, UK; thomas.bannan@manchester.ac.uk (T.J.B.); john.pyle@atm.ch.cam.ac.uk (J.P.)

³ Facility for Airborne Atmospheric Measurements (FAAM), Cranfield University, Building 125, Cranfield, Bedford MK43 0AL, UK; sbau@nerc.ac.uk

⁴ Department of Earth Sciences, Royal Holloway, University of London, Egham TW20 0EX, UK; d.lowry@es.rhul.ac.uk (D.L.); r.fisher@es.rhul.ac.uk (R.F.); j.france@uea.ac.uk (J.F.); e.nisbet@es.rhul.ac.uk (E.N.)

⁵ School of Chemistry, University of Bristol, Cantock's Close, Bristol BS8 1TS, UK; d.e.shallcross@bristol.ac.uk

* Correspondence: carl.j.percival@jpl.nasa.gov; Tel.: +1-818-354-5581

† Current address: Jet Propulsion Laboratory, 4800 Oak Grove Drive, Pasadena, CA 91109, USA.

Received: 25 November 2016; Accepted: 13 June 2017; Published: 22 June 2017

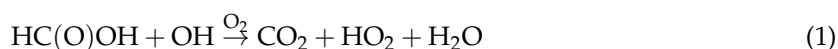
Abstract: This study presents the first gaseous formic acid (HC(O)OH) concentration measurements collected over the Fenno-Scandinavian wetlands (67.9–68.0° N, 22.1–27.8° E) as part of the MAMM (Methane and other greenhouse gases in the Arctic-Measurements, process studies and Modelling) aircraft campaigns conducted in August and September 2013. A boundary layer box model approach has been used to calculate a regionally representative (~240 km²) surface flux for HC(O)OH of 0.0098 (±0.0057) mg_[HCOOH]·m⁻²·h⁻¹. A surface-type classification map was used to estimate proportional source contributions to the observed HC(O)OH flux over the measurement region. The removal of expected source contributions (using available literature parameterisations) from the calculated surface flux identified that 75% remained unaccounted for. This may suggest that HC(O)OH emission from wetland within the Fenno-Scandinavian region could contribute up to 29 times higher per unit area than previous theoretical HC(O)OH globally-averaged wetland estimates, highlighting a need for further constrained wetland studies of HC(O)OH emission to better understand its potentially significant impact on the Arctic HC(O)OH budget and consequent impacts on oxidative capacity.

Keywords: formic acid; CIMS; aircraft measurements; Arctic; wetland; soils

1. Introduction

Formic acid (HC(O)OH) is considered to be the most abundant carboxylic acid, ubiquitous in the atmosphere. It has been detected in the gaseous [1], liquid [2] and the particulate phases [3] and seen across urban [4], rural [5] and marine environments [5]. It is considered to be a significant component of rain water acidity in remote regions, thereby influencing pH dependent aqueous reactions [3]. Aerosol containing HC(O)OH can act as efficient cloud condensation nuclei (CCN), contributing to

the total aerosol loading and thereby influencing the total indirect radiative forcing on the planet [5]. Gaseous HC(O)OH can also influence the oxidative capacity of the atmosphere by the removal of hydroxyl radicals via reaction Equation (1) [6].



Current global models have been found to substantially under-predict HC(O)OH levels in the high latitudes [7,8], and although numerous sources have been identified, their relative contribution remains highly uncertain. Source types include direct emissions from anthropogenic and biogenic processes, and secondary production via alkene ozonolysis [9,10]. The dominant sources in the high latitudes are expected to be tree [11] and soil emission [12], vehicle emission [4,13,14], long range transport of biomass burning emission [15], and ocean emission [5,16]. Previous studies have suggested oceanic algae may also contribute [5,17], however the lack of understanding of the mechanism, reaction pathways, and the large range of different algae species means that the assessment of algae emission is particularly challenging. The principal sinks for HC(O)OH are wet and dry deposition, thus the atmospheric lifetime for HC(O)OH is estimated to be 1.6 days in the boundary layer and approximately 3.2 days in the free troposphere [5].

1.1. Arctic Wetland Source of HC(O)OH

HC(O)OH concentrations in the high latitudes have shown elevated levels in the summer which would suggest the missing source contributions to modelled HC(O)OH predictions are likely to be of biogenic origin [7,18]. One such source yet to be quantitatively evaluated is potential emission from wetland soils. Soil bacteria are a well-documented source of HC(O)OH and an active component in wetlands [19]. To our knowledge, no emission flux studies have previously been undertaken, measuring direct HC(O)OH emission from wetlands. Paulot et al. [5] suggested that HC(O)OH emission from soil is directly proportional to the emitted NO concentration from the same source. Using the ratio $0.95 \text{ nmol}_{\text{HC(O)OH}} \cdot \text{nmol}^{-1}_{\text{(NO)}}$ obtained from data collected over dry savannah soil [12], and globally-modelled NO data collected over known regions of wetlands, Paulot et al. [5] inferred a globally-averaged HC(O)OH emission factor of $2.5 \times 10^{-4} \text{ mg}_{\text{[HCOOH]}} \cdot \text{m}^{-2} \cdot \text{h}^{-1}$ at 303 K for wetland soils. The wet conditions associated with wetland soils are expected to reduce HC(O)OH emission, whereas increased soil acidity and soil temperature are likely to promote emission, although field studies are clearly required to assess these theories [5]. The mean surface temperatures in the high northern latitudes have been shown to increase at twice the rate of the global average over the last 20 years, and these higher temperatures are expected to continue to rise in the future [20,21]. Although HC(O)OH emission from wetlands is poorly understood at present, the increasing temperatures in the Arctic are likely to have significant consequences for temperature dependent sources such as Arctic wetland soils. Wetland is considered the most biologically diverse of all ecosystems and represents a broad spectrum of different types of environments, which include swamps, marshes, bogs and fens, therefore it is apparent that wetlands must be assessed based on their specific environment. Wetlands are defined based on three components; soil, vegetation and hydrology [22]. Of these components, vegetation and hydrology are sensitive to daily conditions, as well as seasonal climatic fluctuations. It is these components that are likely to influence the processes governing HC(O)OH emission. The high affinity of HC(O)OH to water would suggest high levels of water content are likely to reduce or prohibit HC(O)OH emission, therefore hydrology is likely to have a significant role in the process. The Fenno-Scandinavian region spanning Finland and Sweden represents one of the largest wetland areas in Europe and thereby a potentially significant source of HC(O)OH impacting the Arctic atmosphere. As temperatures rise in the high latitudes and the ground thaw reaches greater soil depths, organic chemical species within the wetland soil are likely to become more available for release into the atmosphere [23]. Organic matter tends to accumulate in wetland soils to a greater extent than upland soils because of its high rate of production relative to its rate of decomposition [24]. Furthermore, SoilGrids1KM [25] estimates the Fenno-Scandinavian

wetlands to be organically rich (100–300 g·kg⁻¹ organic carbon content) and estimates a mean soil pH ranging between 4.6 and 5.6. Based on previous wetland estimates, these conditions may be considered favourable for the release of HC(O)OH [5]. HC(O)OH emissions in the Fenno-Scandinavian wetlands however, have not been evaluated and the magnitude of this source to the regional budget remains unknown. This study represents the first flux derived from gaseous HC(O)OH measured concentrations over a wetland region in the Fenno-Scandinavian Arctic, with a view to assessing the impact of wetlands on the regional HC(O)OH budget.

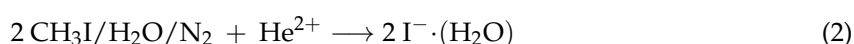
1.2. Campaign Outline

As part of the MAMM (Methane and other greenhouse gases in the Arctic-Measurements, process studies and Modelling) aircraft campaign, measurements were collected within the Fenno-Scandinavian Arctic, a region proportionally occupied by wetlands. The data presented in this study incorporate two aircraft campaigns based out of Kiruna, Sweden during the periods of 15–18 August and 19–23 September 2013. These were used to derive HC(O)OH mass budget fluxes, with the aim of understanding and reducing the uncertainty of regional emission sources with a particular focus on the Fenno-Scandinavian wetlands.

2. Experimental

2.1. CIMS Measurement Technique

A Chemical Ionisation Mass Spectrometer (CIMS) (Georgia Institute of Technology, Atlanta, GA, USA) was deployed for in-situ measurement of HC(O)OH on board the FAAM BAe-146 research aircraft at a frequency of 1 Hz. The CIMS instrument was constructed by Georgia Institute of Technology as described by Nowak et al. [26] and set up on the FAAM BAe-146 aircraft as described by Le Breton et al. [9]. This technique utilised iodide anions for the detection of HC(O)OH as described by Slusher et al. [27]. This method followed the same procedure as described by Le Breton et al. [9] and Jones et al. [17] whereby a flow of methyl iodide (CH₃I) gas mixture was passed over a radioactive ²¹⁰Po source, initiating a dissociative electron attachment reaction with CH₃I to form the reagent anion I⁻·(H₂O) as shown by Equation (2). This anion is passed into the ion molecule region where it combines with HC(O)OH and HCN species via the adduct reactions Equations (3) and (4), to enable detection of HC(O)OH at *m/z* = 173 (I⁻·HC(O)OH) and HCN at *m/z* = 154 (I⁻·HCN). For further details on sampling method, please refer to Le Breton et al. (2012).



2.2. Formic Acid and HCN Calibration

Following the same approach as Jones et al. [17], water-specific background calibrations were performed for HC(O)OH and HCN before each flight. Set flows of dry N₂ (ranging 0–7380 SCCM dry N₂) were combined with scrubbed ambient air, which altered the I⁻·H₂O ion counts, as well as the I⁻·HC(O)OH and I⁻·HCN background signal. These measurements produce a linear relationship between I⁻·H₂O ion counts and the detected ion signal for the species; I⁻·HC(O)OH and I⁻·HCN. This linear relationship is then applied to the measured data to produce a water-corrected instrument background signal of each species for each data point. Water-specific HC(O)OH sensitivity calibrations were also performed at the start, mid-point and end of the campaigns, to determine the HC(O)OH sensitivity corresponding to the I⁻·H₂O signal. Firstly, a water-specific background calibration was conducted to establish the water-corrected instrument background for HC(O)OH. Secondly a HC(O)OH gas standard was added (10 SCCM) to a set flow of scrubbed ambient air (7380 SCCM),

where the change in $I^- \cdot HC(O)OH$ counts from its background is used to calculate a sensitivity. $I^- \cdot H_2O$ counts are then altered by the addition of set flows of dry N_2 where the $HC(O)OH$ sensitivity change is monitored in relation to the change in $I^- \cdot H_2O$ counts. This calibration shows a linear relationship between $I^- \cdot H_2O$ counts and $HC(O)OH$ sensitivity. $HC(O)OH$ gas mixtures were prepared using a custom-made manifold and cylinder concentrations were validated after the campaigns using GC-FID analysis. This methodology is described in greater detail by Jones et al. [17].

HCN was calibrated relative to that of $HC(O)OH$, where the sensitivity of HCN was determined from laboratory calibrations, where a flow of 5 SCCM (BW Technologies HCN calibration cylinder, 10 ppm) was diluted in a flow of ambient air at a stable count of $\sim 670,000$ for $I^- \cdot H_2O$ signal, $m/z = 145$. A second laboratory calibration was performed for $HC(O)OH$, equivalent to the same concentration as HCN in the same conditions at approximately $670,000 I^- \cdot H_2O$ signal. This equated to a sensitivity ratio of 24:1 at $I^- \cdot H_2O$ equal to $670,000$ counts. HCN sensitivity was found to be independent of $I^- \cdot H_2O$ counts. Therefore, HCN ion count data were normalised for the campaigns based on $HC(O)OH$ sensitivity at $670,000 I^- \cdot H_2O$ counts.

2.3. CH_4 Measurements (FGGA and WAS Sampling)

In-situ CH_4 measurements (1 Hz) were obtained using a commercially available cavity-enhanced absorption spectroscopy (CEAS, Model RMT-200, Los Gatos Research Inc., San Jose, CA, USA) that was modified for aircraft use O'Shea et al. (2013) provides a full description of the configuration of this instrument on board the FAAM Bae-146 research aircraft, together with the associated data processing and quality control. CH_4 uncertainty is calculated at ± 1.3 ppb; 1 Hz precision is ± 2.5 ppb [28]. Measurements of CH_4 were also made by analysing whole air samples using cavity-ring down spectroscopy (Model G1301, Picarro Inc., Santa Clara, CA, USA). The mean bias of the whole air samples (400 samples) relative to the in-situ measurements was -0.5 (1 standard deviation = 4.6) ppb for CH_4 . Whole Air Samples (WAS) were collected in stainless steel flasks as described by Lewis et al. [29] and analysed post-flight in the laboratory for the $\delta^{13}C$ isotopic ratio of CH_4 . The $\delta^{13}C$ (CH_4) isotopic signature analysis was performed by continuous-flow gas chromatography/isotopic-ratio mass spectrometry (CF-GC-IRMS), with a precision of 0.1% , to derive a Keeling plot [30,31], and used to interpret the dominant source type.

2.4. CO , O_3 and Additional Supporting Measurements (FAAM BAe-146 Core Instruments)

CO concentration measurements are collected on board the FAAM BAe-146 aircraft using an AL 5002 VUV Fast Fluorescence CO Analyser (Aero-Laser GmbH, Garmisch-Partenkirchen, Germany) with an uncertainty of $\pm 5\%$ [32]. O_3 data were collected by a TE49C UV Photometric Ozone Analyser (Thermo-Fischer Scientific, Waltham, MA, USA) as part of the core instrumentation on board the aircraft, with an uncertainty of ± 3 ppb [33]. Relative humidity is calculated on the aircraft by the FAAM CORE General Eastern GE 1011B Chilled Mirror Hygrometer. Additionally, temperature was recorded using the FAAM CORE Rosemount/Goodrich type 102 Total Air Temperature sensors [34].

3. Flux Calculation

Previously, aircraft mass budget calculations have been performed successfully to derive regionally representative fluxes of trace species [34–39]. For this approach to be applicable, the composition of the air inflow-outflow to a particular region needs to be characterised to determine the enhancement of a species associated with a given region. We employ the same approach as O'Shea et al. [34], whereby measurements are collected along the prevailing wind vector. If it can be assumed that within the PBL (with depth Z_1) no vertical gradients exist in the species of interest, a net flux of the species S can be determined as shown by Equation (5).

$$flux = \frac{\bar{U}}{\cos \theta} \frac{dS}{dx} \int_0^{Z_1} n dz \quad (5)$$

\bar{U} ($\text{m}\cdot\text{s}^{-1}$) represents the mean wind speed, and n ($\text{molecules}\cdot\text{m}^{-3}$) is the atmospheric number density, which is integrated from the surface to the top of the PBL (dz). The dS ($\text{molecules}\cdot\text{molecules}^{-1}$) term represents the species enhancement for “S” over the distance $\cos\theta \cdot dx$ parallel to the prevailing wind, where θ is the difference between the mean wind vector and the direction taken by the aircraft along transect x . This enhancement is represented by a concentration gradient determined by averaging the data to 30 s intervals along transect x . The measured variation in the wind speed, HC(O)OH concentration gradient in relation to distance x , wind direction and boundary layer height, defined as one times the standard deviation (1σ) of each term, and are used to calculate an overall flux uncertainty for each flux estimate.

4. Case Studies

4.1. Case Study B796b

On 16 August 2013 (Flight B796b), the FAAM BAe-146 aircraft performed an east-to-west transect (transect x) at 14:41:00 to 15:14:30 UTC between the coordinates 68.0° N, 27.9° E and 68.0° N, 22.1° E taking concentration measurements over the Fenno-Scandinavian wetlands. Transect x was conducted over a distance of 239 km at an approximate altitude range of 444 m to 721 m within the planetary boundary layer (PBL) at an average temperature (± 1 times the standard deviation) of $283.1 (\pm 1.2)$ K. The east–west transect was carried out at an angle of $92.6 (\pm 2.6)^\circ$ which was roughly aligned against the prevailing wind bearing of $315.6 (\pm 26.5)^\circ$. The data obtained were reversed in terms of direction to align with the wind direction to ascertain the angle alignment difference of 41.1° , used in the flux calculation. The mean wind speed during transect x was calculated as $2.9 (\pm 0.9) \text{ m}\cdot\text{s}^{-1}$, as shown in Table 1. This calculation assumes the near-surface emissions are immediately mixed throughout the PBL. Therefore, to validate this assumption, the time taken for air to advect across transect x must be significantly greater than the PBL turnover time.

Following the same approach as Karion et al. [40], the mean PBL turnover time (t_t) for species to mix from the surface to the top of the boundary layer, can be estimated by $t_t = Z_1/w^*$, where Z_1 is the PBL height and w^* is the convective velocity scale. The convective velocity scale is calculated using Equation (6).

$$w^* = \left(\frac{gZ_1 \overline{w'\theta_V'}}{\bar{\theta}_V} \right)^{1/3} \quad (6)$$

In relation to Equation (6), g signifies the standard acceleration due to gravity at the Earth’s surface ($9.8 \text{ m}\cdot\text{s}^{-2}$), $\overline{w'\theta_V'}$ is the surface buoyancy flux ($0.0191 \text{ K}\cdot\text{m}\cdot\text{s}^{-1}$), and $\bar{\theta}_V$ (284 K) represents the mean virtual potential temperature obtained from the profile ascent (in this case between 13:33–13:42 UTC). The surface buoyancy flux data were collected from the Sodankylä ground research site located at coordinates 67.369° N, 26.654° E, at time 13:30 UTC. Based on this calculation the PBL turnover time was estimated to be ~ 22 min. This is significantly shorter than the time taken for air to advect across transect x (~ 22 h and 53 min). Therefore, the assumption that emissions are immediately mixed throughout the PBL over the length scale of transect x can be considered reasonable.

The PBL height during transect x was derived from potential temperature data recorded by thermodynamic instrumentation on flight B796b, using the ascent and descent vertical profiles at 13:33–13:42 UTC and 17:23–17:32 UTC, respectively. In examining the ascent profile shown in Figure 1, a strong increase in potential temperature is apparent at 1460 m, indicative of the top of the PBL. This profile was obtained between the coordinates 67.8° N, 20.3° E and 68.3° N, 21.1° E, relatively close to the edge of the region in which the flux was calculated. Furthermore, the second vertical profile

identified a clear elevation in potential temperature at 1200 m. This was obtained between similar coordinates of 67.5° N, 20.7° E and 67.8° N, 20.3° E later in the day. For the purpose of this calculation a PBL top of 1330 (± 130) m was chosen as the mean altitude between the two profiles. The potential temperature profiles show little structure between the ground and PBL top supporting our implicit assumption of a well-mixed boundary layer.

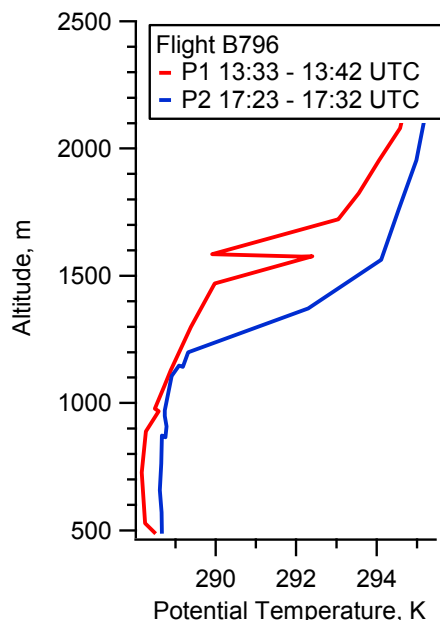


Figure 1. The potential temperature change experienced by changing altitude during flight B796b's profile ascent (P1) at time 13:33–13:42 UTC and the profile descent (P2) at time 17:23–17:32 UTC identifying clear temperature increases at 1460 and 1200 m, respectively.

4.2. Case Study B797

Following the approach described in Section 2.2, two transect-average flux concentration measurements of HC(O)OH were obtained from flight B797 on the 17 August 2013 over the Fenno-Scandinavian wetlands and used to calculate an overall flux. The first flux measurement was recorded between the coordinates 67.9° N, 26.6° E and 68.0° N, 24.5° E following an east-to-west trajectory over a distance of ~78 km at 08:31:30–08:43 UTC. The average wind direction of 331 (± 7)° was aligned against the aircraft bearing of 87 (± 5)°. Following the same approach to flight B796b, 180° was added to the aircraft bearing in order to ascertain the alignment difference (63°) between the prevailing wind and the aircraft bearing. The average wind speed during this transect was 6.2 (± 0.5) m·s⁻¹ at an average temperature of 283.7 (± 0.5) K comparable with flight B796b conditions.

The second set of data was obtained on flight B797 over the same region, between coordinates 68.0° N, 24.5° E and 68.0° N, 28.0° E at 08:45–09:07:30 UTC, travelling a distance of ~147 km in a west-to-east direction. The average wind speed during this period was 5.8 (± 0.6) m·s⁻¹, with an average temperature of 284.1 (± 0.4) K. An average wind direction of 348.6 (± 11.9)° was aligned within a 90° angle to the aircraft bearing of 269.3 (± 15.0)°, resulting in an angle difference of 79.3°. The two data sets were collected over the same latitude and longitude, with a minimal time difference between runs. Therefore, to provide a more representative flux, the data sets were combined to calculate an overall flux. Potential temperature data obtained from a descent profile flight on B797 were used to estimate a PBL top of 1310 m with an uncertainty of ± 100 m, as shown in Figure 2.

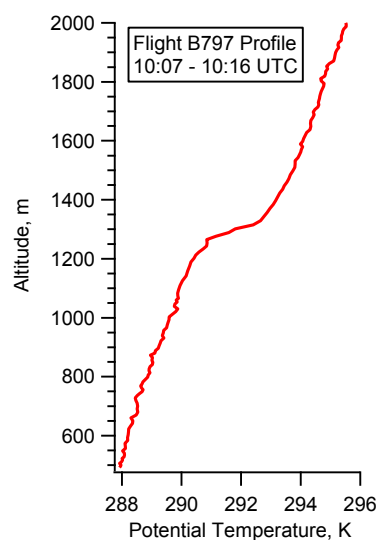


Figure 2. The potential temperature change experienced during flight B797's ascent at time 10:07–10:16 UTC, where a large temperature increase is observed at ~1310 m altitude.

4.3. Case Study B804

The second MAMM aircraft campaign was conducted in September 2013, where an additional HC(O)OH flux measurement was completed on 19 September 2013 during flight B804. Measurements were taken over the same wetlands region as the previous flights, and followed a west-to-east transect between the coordinates 68.0° N, 25.1° E and 68.0° N, 26.7° E at 16:59:30–17:10:30 UTC. The average temperature during this flight was 283.1 (± 0.5) K, comparable to the previous flux measurements, and the average wind speed was 9.3 (± 1.1) $\text{m}\cdot\text{s}^{-1}$. An average wind direction of 310 (± 6)° during these measurements was aligned almost parallel with the aircraft bearing of 273 (± 4)° along transect x , resulting in an angle alignment difference of 37°. Potential temperature data obtained from this flight between 17:10 and 17:17 UTC, revealed a strong increase at approximately 1475 m as shown by Figure 3. Therefore, the PBL top was estimated to be 1475 (± 100) m and represented suitable conditions to calculate a flux estimate.

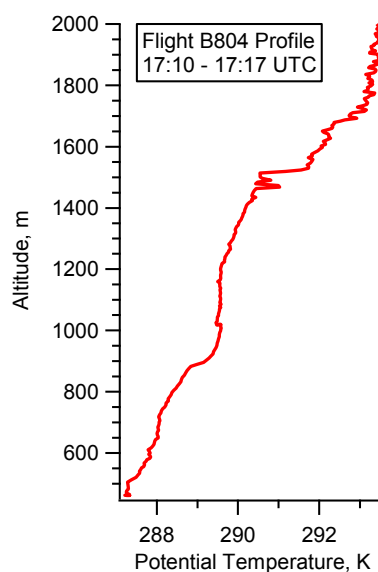


Figure 3. The potential temperature change experienced during flight B804's ascent at time 17:10–17:17 UTC, where a large temperature increase is observed at 1475 m altitude.

5. Results and Discussion

5.1. Flight B796b: HC(O)OH Flux

This study recorded a HC(O)OH concentration change of approximately 143 ppt ranging from a low of ~120 ppt to a high of ~262 ppt with a R^2 of 0.5, as shown by Figure 4. Using Equation (5), the calculated HC(O)OH emission flux over the Fenno-Scandinavian wetlands region was estimated to be $0.0098 (\pm 0.0057) \text{ mg}_{[\text{HCOOH}]} \cdot \text{m}^{-2} \cdot \text{h}^{-1}$ on 16 August 2013. The uncertainty in the total flux was determined by propagating the uncertainties associated with the individual terms. The individual uncertainties and total uncertainties associated with each case study are illustrated in Table 1. These included the uncertainties in the observed (fitted) HC(O)OH concentration gradient, the known variability in the wind speed, wind direction and the boundary layer mixing height. HCN concentrations for transect x were comparatively low at $64 (\pm 17)$ ppt. Following the same approach by Le Breton et al. [41], the 6-sigma method for identifying airmasses of biomass burning origin was applied to the HCN measurements from flight B796b. This method identified an airmass with a HCN concentrations exceeding 109 ppt would be indicative of a biomass burning plume. HCN concentrations during this flight were no greater than 102 ppt suggesting the observed airmass during the flux measurement contained no biomass burning influence. CO and O₃ concentrations remained relatively constant at background levels of $83.9 (\pm 0.4)$ ppb and $29.1 (\pm 0.9)$ ppb respectively as shown by Figure 5. No rainfall occurred during these measurement periods thereby removing the effect of wet deposition, which would suggest suitable conditions for capturing a surface emission flux.

The mean relative humidity during this transect was $82.5 (\pm 8.4)\%$. Interestingly, relative humidity revealed a partial correlation with HC(O)OH concentrations ($R^2 = 0.45$) along transect x , with an observed sharp decrease of 26.5% from approximately 24.2° E to 26.1° E longitude, as shown by Figure 6. This sharp decrease in relative humidity may represent a potential loss mechanism for gaseous HC(O)OH via uptake onto water vapour droplets. However, a recent study by Veres et al. [42] revealed gaseous HC(O)OH concentrations were relatively unchanged under a range of controlled relative humidity conditions (ranging between 0% and 100% relative humidity), therefore for the purpose of this flux calculation this potential loss pathway was not considered.

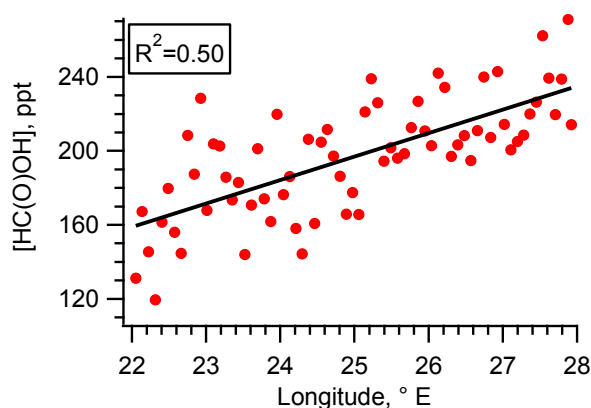


Figure 4. Represents the concentration change in HC(O)OH as the aircraft travelled east along transect x during flight B796b on 16 August 2013.

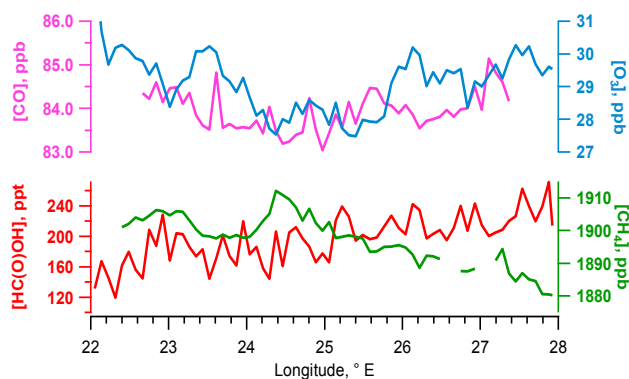


Figure 5. The concentration change in HC(O)OH, CH₄, CO and O₃ along transect *x* in relation to longitude in ° E during flight B796b on 16 August 2013.

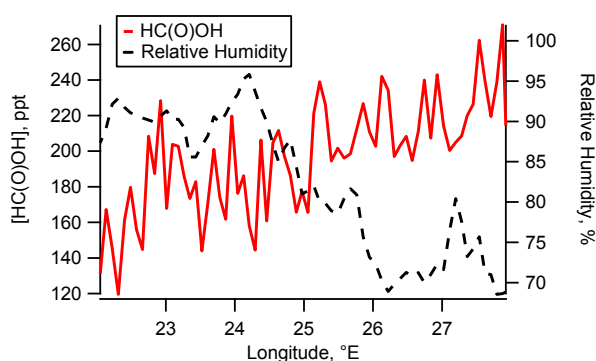


Figure 6. The change in HC(O)OH concentration and relative humidity in relation to longitude, ° E along transect *x* during flight B796b on 16 August 2013.

Methane (CH₄) is a well-documented emission from wetlands to the atmosphere [34,43] and represents a useful tracer for wetland emissions. Regional methane sources from wetlands have successfully been identified through Keeling plot analysis of $\delta^{13}\text{C}$ in CH₄ from WAS samples [43–45]. Methane measurements and WAS samples were also collected during the same observation period. The resulting Keeling analysis revealed a source signature of $-72.8 \pm 1.9\text{‰}$, as displayed by Figure 7. Based on previously measured source analyses over the Fenno-Scandinavian wetlands during the summer, this $\delta^{13}\text{C}$ (in CH₄) source signature is within the expected range (-75 to -69‰) for a high northern latitude wetland CH₄ emission source, thereby adding further credence to the suggestion of a wetland source contributing to the observed HC(O)OH flux. Figures 5 and 8 illustrate HC(O)OH concentrations partially anti-correlate with CH₄ concentrations along transect *x* with an R² of 0.37. Influences from sources unique to the individual species may explain these observations. Additionally, several strains of methanogens have been found to use HC(O)OH as a substrate for producing CH₄ [46] which may contribute to the detected anti-correlation. CH₄ emissions from wetlands are expected to be greater in saturated soil conditions [47], whereas gaseous HC(O)OH emissions are likely to be reduced in saturated conditions due to the hydrophilic properties of HC(O)OH. Therefore, the effects of water may also play a crucial role in governing the emission processes of these species. Constrained laboratory studies monitoring the effect of soil moisture content on HC(O)OH emission would be required to test this hypothesis.

Table 1. The mean average values for the term variables used in the flux calculation, as well as one times the standard deviation (1σ) of the mean value used to calculate the overall flux uncertainty.

Parameter	B796b		B797 (Combined)		B804	
	Mean Value	Variability (1σ)	Mean Value	Variability (1σ)	Mean Value	Variability (1σ)
Wind Speed (U)	2.9 $\text{m}\cdot\text{s}^{-1}$	$\pm 0.9 \text{ m}\cdot\text{s}^{-1}$	5.9 $\text{m}\cdot\text{s}^{-1}$	$\pm 0.6 \text{ m}\cdot\text{s}^{-1}$	9.3 $\text{m}\cdot\text{s}^{-1}$	$\pm 1.1 \text{ m}\cdot\text{s}^{-1}$
Wind direction	315.6°	$\pm 26.5^\circ$	342.4°	$\pm 13.5^\circ$	309.9°	$\pm 5.6^\circ$
Alignment difference between flight track and wind component ($\cos\theta$)	0.731	0.315	0.280	0.227	0.796b	0.076
[HC(O)OH] enhancement over transect x from background	143 ppt	$\pm 30 \text{ ppt}$	51 ppt	$\pm 12 \text{ ppt}$	-40 ppt	$\pm 10 \text{ ppt}$
HC(O)OH enhancement vs transect x longitude (R^2 fit)	0.51		0.03		0.08	
Boundary Layer Height (Z_1)	1330 m	$\pm 130 \text{ m}$	1310 m	$\pm 100 \text{ m}$	1475 m	$\pm 100 \text{ m}$
Total Flux ($\text{mg}\cdot\text{m}^{-2}\cdot\text{h}^{-1}$)	0.0098	± 0.0057	0.0096	± 0.0079	-0.0146	± 0.0029

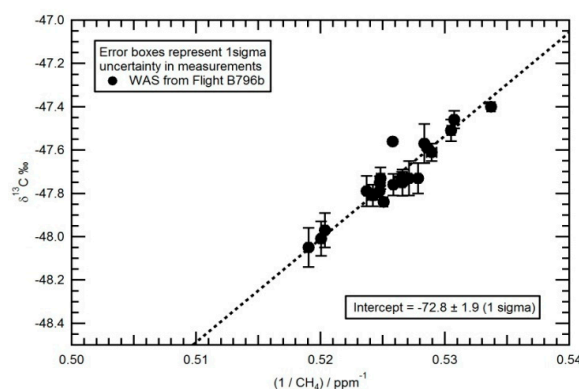


Figure 7. Keeling plot of the WAS data set obtained between 14:40:00 and 15:14:30 during flight B796b and a background sample (10 min prior to transect x). The y -axis intercept gives the isotopic signature of the “added” methane over the background.

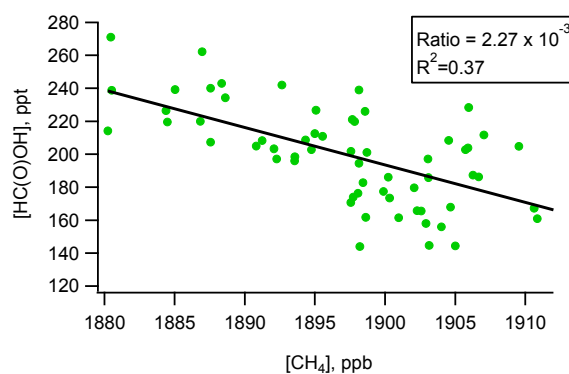


Figure 8. The relationship between the concentrations of HC(O)OH and CH_4 , along transect x during flight B796b on 16 August 2013.

Source Attribution

To address the influence from other known sources of HC(O)OH, an underlying surface-type classification map [48], was used to identify the vegetation and land use types within the flight transect area, as detailed in Table 2 and illustrated in Figure 9. This map characterised the sampling region for flight B796b to consist of coniferous forests (26.9%), peat bogs (24.3%), mixed forests (22.2%),

woodland shrub (12.2%), water bodies (7.1%), broad-leaf forest (5.1%), moors and heathland (1.8%), water courses (0.3%) and pastures and agricultural land (0.1%). In order to hypothesise the contribution of other sources in the measurement region, emission factors of known sources were deducted from the flux estimate.

Although not a conclusive measure, this method offers insight into possible contributions of un-quantified sources such as wetlands or of sources not yet known. Established emissions sources in the region include tree emission and soil emission. The dominant tree species in this region of Fenno-Scandinavia is the Norwegian Spruce tree, a well-established source of HC(O)OH with a standard emission factor of $0.0040 \text{ mg}_{[\text{HCOOH}]} \cdot \text{m}^{-2} \cdot \text{h}^{-1}$ [11]. Assuming coniferous and mixed tree areas (49.1%) are entirely occupied by Norwegian Spruce trees and the emission factor is independent of temperature, we can assume an emission factor contribution (49.1%) from tree species of $0.0020 \text{ mg}_{[\text{HCOOH}]} \cdot \text{m}^{-2} \cdot \text{h}^{-1}$. Furthermore, soil is another well-known source of HC(O)OH emission and based on Figure 9 and Table 2, there is likely a strong contribution from soil emission in the flux region. Paulot et al. [5] devised a temperature dependent calculation for estimating a HC(O)OH emission factor from soil as shown below, where T is expressed in Celsius for this calculation.

$$[\text{HC(O)OH}]_{\text{soil}} = (0.0017 \times e^{(0.119 T - 1)}) \quad (7)$$

Based on the average temperature recorded during concentration measurements along transect x (283 K, 10 °C), this study hypothesises a soil emission factor of $6.4 \times 10^{-4} \text{ mg}_{[\text{HCOOH}]} \cdot \text{m}^{-2} \cdot \text{h}^{-1}$ in this region. In this discussion, we assume a soil contribution of 68.3%, resulting in an overall estimated contribution of $4.4 \times 10^{-4} \text{ mg}_{[\text{HCOOH}]} \cdot \text{m}^{-2} \cdot \text{h}^{-1}$. This assumes all land represents soil emission of HC(O)OH except for areas identified with a water surface (Table 2; peat bogs: 24.3%, water bodies: 7.1% and water courses; 0.3%). The estimated emission factors used in this investigation are likely to represent an overestimation of their contribution to the observed flux. However, by deducting these emission factors in proportion to their percentage contribution, an estimated $0.0074 \text{ mg}_{[\text{HCOOH}]} \cdot \text{m}^{-2} \cdot \text{h}^{-1}$ remains unaccounted for, and the hypothesis is that wetland emission may contribute much more significantly than previously thought. Paulot et al. [5] estimates a wetland contribution of $2.5 \times 10^{-4} \text{ mg}_{[\text{HCOOH}]} \cdot \text{m}^{-2} \cdot \text{h}^{-1}$, less than 4% of the residual emission rate observed in these measurements, thus suggesting wetlands or other sources, not yet known, may be contributing significantly to the observed flux.

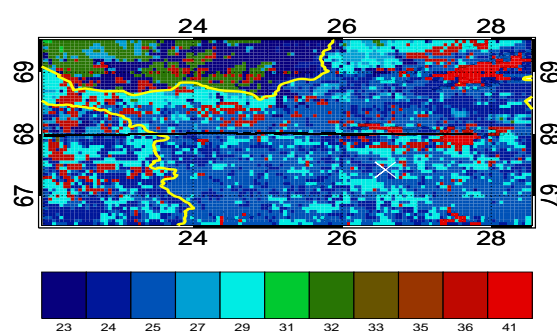


Figure 9. Underlying surface-type classification map [48] used to identify prevalent vegetation and land use types within transect x for flights B796b, B797 and B804, within the coordinates of 67.5° – 68.5° N and 22.1° – 27.9° E. The white cross is used as a reference point to identify the town of Sodankyla in Finland, and the yellow markings signify the borders between Sweden (**left**), Norway (**top**) and Finland (**right**). The black line represents the specific flight path for B796b and the colour coded legend is identified in Table 2.

Table 2. The key for the numbers and colours associated with underlying surface-type classification map (Figure 9), which is used to identify prevalent vegetation and land use types within transect *x* for flight B796b.

Number	Land Type	Surface-Type Proportion Occupying Transect <i>x</i> in the Flight Track for B796b, %
18 *	Pastures	0.02
21 *	Agricultural land with significant natural vegetation	0.05
23	Broad-leaf forest	5.1
24	Coniferous forest	26.9
25	Mixed forest	22.2
27	Moors and heathland	1.8
29	Woodland shrub	12.2
31	Bare rocks	0
32	Sparsely vegetated areas	0
33	Burnt areas	0
35 *	Inland marshes	0.002
36	Peat bogs	24.3
40 *	Water courses	0.3
41	Water bodies	7.1

* Represents surface types within the flight track for transect *x* that were too small to be observed on the classification map illustrated in Figure 9.

5.2. Flight B797: HC(O)OH Flux

The combined data for flight B797 were used to calculate an overall flux emission rate of $0.0096 (\pm 0.0079) \text{ mg}_{[\text{HCOOH}]} \cdot \text{m}^{-2} \cdot \text{h}^{-1}$, using the same approach as the flux emission rate calculated for case B796b. Given the difficulties associated with changing meteorological conditions for calculating a flux over the same region between consecutive days, the agreement between flux concentration measurements is excellent. HCN concentrations remained low throughout this transect with an average concentration of 44 (± 17) ppt. Furthermore, HCN concentrations remained below the 6-sigma threshold of 88 ppt, suggesting the air mass was not influenced from biomass burning [41]. The HC(O)OH concentration gradient in this flux ranged from a low of 186 ppt in the west to 247 ppt in the east, with an average concentration of 215 (± 12) ppt. Concentrations are within a similar range and follow the same trend as the previous flight, with larger concentrations in the east, downwind of the Fenno-Scandinavian wetlands. The concentration change in this flight, however, was much more variable resulting in an R^2 of only 0.03, significantly less than for the previous case (flight B796b). O_3 concentrations followed a similar trend to HC(O)OH, increasing across the west-to-east transect, with a mean of 26.4 (± 1.8) ppb. A HC(O)OH enhancement was also observed at longitude 26.5° E correlating with a 6 ppb rise in O_3 , which could be indicative HC(O)OH production via ozonolysis, however without additional NO_x measurements this process cannot be investigated further. Alternatively, based on the overlaying land map of the region, this area at longitude 26.5° E is classified as the largest area occupied by wetlands, and instead may represent the largest contribution from wetlands emission. The average CO concentration was relatively low at 89.2 (± 1.2) ppb during the flight, suggesting local anthropogenic pollution was minimal. The angle difference between the average wind direction and the average aircraft bearing during flight B797 concentration measurements was 74°. Although this is considered in the flux calculation and uncertainty, the magnitude would suggest that the HC(O)OH concentrations were not directly downwind of transect *x*, and thus likely influenced by additional sources from outside of the associated flux region. Therefore, considering these uncertainties, flight B797's flux has been included qualitatively in this study to investigate repeatability within the flux concentrations between consecutive days and to better interpret local sources within transect *x*. Despite this, HC(O)OH concentrations followed a similar concentration range and trend observed in flight B796b, increasing in the eastern area of the measurement region.

$\delta^{13}\text{C}$ (CH_4) analysis of 10 WAS bottles collected during flight B797, including one sample taken along transect *x*, produced a Keeling plot isotopic signature of $-71.1 \pm 0.6\text{‰}$. This is in excellent

agreement with isotopic source signatures of boreal wetland emission from this region. As shown in Figure 10a,b, CH₄ measurements did not correlate with HC(O)OH levels, particularly after longitude 26° E, similar to observations from flight B796b. The mean relative humidity during this combined flux measurement was 87.7 (±2.6)%, and remained relatively unchanged throughout this transect with no correlation with HC(O)OH measurements, suggesting stable conditions. No rainfall occurred during measurements, thus indicating HC(O)OH loss via wet deposition was insignificant. Although there remains a high degree of uncertainty in this second flux estimate, the similarity in HC(O)OH levels between this flux measurement and flight B796b (within a day of each other) adds further credence to the suggestion that these observations are the result of a relatively local source.

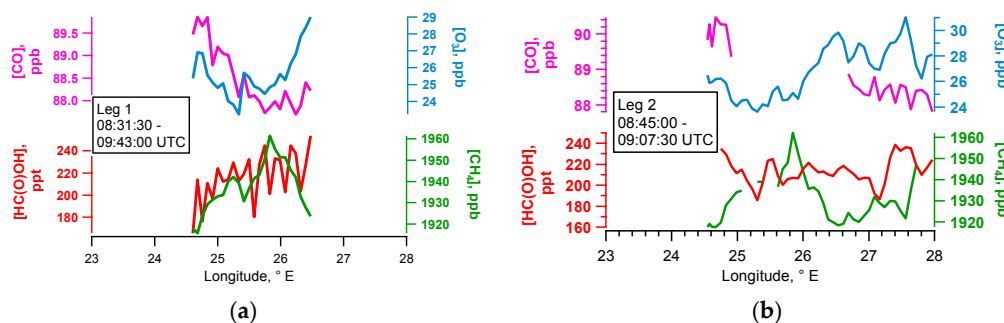


Figure 10. The concentration trend for HC(O)OH, CH₄, O₃ and CO travelling; (a) ~78 km along transect *x* during flight B797 at 08:31:30–08:43 UTC (leg 1), (b) ~147 km along transect *x* during flight B797 at 08:45–09:07:30 UTC (leg 2).

5.3. Flight B804: HC(O)OH Flux

Aircraft measurements were collected between longitudes 23.8° E and 26.7° E, however the data taken between 23.8° E and 25.0° E longitudes revealed sharp enhancements in O₃ (~6 ppb), CH₄ (~12 ppb) and CO (~6 ppb), as shown by Figure 11. HC(O)OH concentrations were variable and elevated (~60 ppt) between these longitudinal points, with a mean concentration of 98 (±17) ppt. The 6 ppb enhancements of O₃ and CO may suggest an anthropogenic influence on the observed measurements. A four-day HYSPLIT backward trajectory at the peak O₃ and CO levels (at 16:54 UTC) indicated the air mass originated from a southeast direction, passing through central continental Russia. The enhancements in these trace species may suggest influence from an additional direct source (likely of anthropogenic origin) other than the known sources in this region. CH₄ measurements were also found to be initially high, and decreased at longitude 25.0° E. These initial elevations may have interfered with expected background HC(O)OH concentrations. As illustrated in Figure 12, relative humidity measurements were found to shift to a higher average at approximately 25.1° E longitude along transect *x*, suggesting a possible change of air mass. The average O₃ and CO concentrations during the remaining leg of transect *x* (25.1° E and 26.7° E longitudes) were relatively stable with background concentrations of 25.4 (±1.4) ppb and 107.3 (±0.5) ppb respectively. Relative humidity measurements also remained relatively stable for the remaining leg of this transect with no correlation with HC(O)OH measurements and a mean relative humidity of 91.6 (±2.1)%. Therefore, to provide a more representative surface flux over the region, the aircraft measurements were restricted to data collected between the coordinates 68.0° N, 25.1° E and 68.0° N, 26.7° E. From this point, HC(O)OH concentration measurements observed a ~41 ppt decrease from approximately 82 ppt to 41 ppt when travelling from west-to-east along transect *x*, as shown by Figure 12. No rainfall occurred during the measurement period suggesting wet deposition was minimal. HCN measurements remained low throughout transect *x* with an average concentration of 55 (±19) ppt between longitudes 23.8° E and 26.7° E, indicative of no biomass burning influence to the observations. Furthermore, the HCN 6-sigma threshold limit for a biomass burning plume was calculated to be 132 ppt, above the observed

HCN measurements for the transect, suggesting that biomass burning had no significant influence on the observed measurements [41]. The HC(O)OH concentration measurements between the defined longitudes resulted in a near surface flux of $-0.0146 (\pm 0.0029) \text{ mg}_{[\text{HCOOH}]} \cdot \text{m}^{-2} \cdot \text{h}^{-1}$, indicating a reversal of this region from a source to a sink. The concentration gradient obtained during these measurements generated an R^2 value of 0.08, significantly lower than the R^2 value obtained in flight B796b flux calculation. Nevertheless, the processes governing HC(O)OH emission within wetlands are highly uncertain due to a lack of wetland-specific emission measurements. Furthermore, the poorly defined classification of the wetland soils in this region creates further difficulties in understanding the important variables impacting HC(O)OH emission from such sources. It is widely accepted that HC(O)OH emission from savannah soils is temperature dependent, and therefore may represent an important factor governing wetland emission. The temperatures recorded between these flux measurements were relatively unchanged suggesting the change of this wetlands region from a source to a sink is not the result of a temperature influence, although this may represent an additional factor in the emission process yet to be investigated [5,12].

$\delta^{13}\text{C}$ (CH_4) data for WAS samples collected below 1000 m altitude during case study B804 were used to calculate an isotopic source signature of $-66.6 (\pm 7.2)\text{‰}$ using a Keeling plot. The large uncertainty associated with this isotopic source signature is a consequence of the relatively low CH_4 enhancements observed during flight B804. Although this value is higher than the expected isotopic signature range for Fenno-Scandinavian wetlands, there is no isotopic evidence from other flights in this campaign to suggest an alternative $\delta^{13}\text{C}$ (CH_4) emission source. Relative humidity measurements were found to be 9.1% higher on average than case study B796b. Although this is not expected to influence gaseous HC(O)OH levels, the differences observed between these flux concentration measurements might suggest it could be an influencing factor within the wetlands emission process. Surface based measurements over a prolonged period of time would be needed in order to assess such an influence on HC(O)OH emission from wetlands. The lower HC(O)OH concentrations observed during flight B804 in comparison to HC(O)OH concentrations in the previous case studies would suggest the observed flux was not a result of an additional source contribution in the background location but rather a reduction in the dominant emission source. As discussed, HC(O)OH's favourability to partition into the liquid phase in the presence of water would suggest soil moisture content is likely to be an important factor influencing HC(O)OH emission from wetlands. Therefore we hypothesise that a change in soil moisture content is likely responsible for the apparent change of this region from a source to a sink, although this theory cannot be confirmed based on the results collected here.

Ultimately, the transition from a source to a sink for this region, as highlighted between case studies B796b and B804, further complicates our understanding of the HC(O)OH emission process from wetlands soils, however, it would appear that wetlands may represent a potentially significant source contributing to the Arctic HC(O)OH budget.

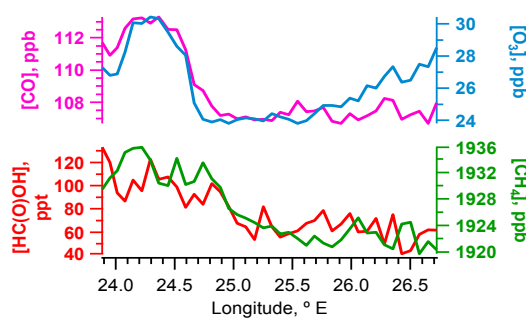


Figure 11. The concentration trend of HC(O)OH, CH_4 , O_3 and CO between the longitudes 23.8° E and 26.7° E along transect x , during flight B804 (19 September 2013), highlighting the variability within the flux between the initial longitudinal points of 23.8° E and 25.0° E .

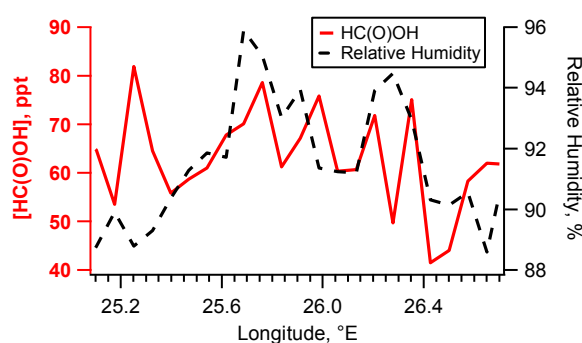


Figure 12. The trend of HC(O)OH concentration (ppt) and relative humidity (%), during the flux measurement period on flight B804 (19 September 2013), between longitudes 25.1° E and 26.7° E along transect *x*.

6. Conclusions

This work presents the first flux derived from gaseous HC(O)OH measured concentrations over a wetland region in the Fenno-Scandinavian area. A best-case scenario (flight B796b) with the most favourable meteorological conditions led to an estimated emission of $0.0098 (\pm 0.0057) \text{ mg}_{[\text{HCOOH}]} \cdot \text{m}^{-2} \cdot \text{h}^{-1}$. The removal of (upper limit estimation) emission factors of known sources in the region (tree and soil emission) from the overall flux calculation revealed $0.0074 \text{ mg}_{[\text{HCOOH}]} \cdot \text{m}^{-2} \cdot \text{h}^{-1}$ still unaccounted for. Due to the lack of knowledge of wetland HC(O)OH production processes and release pathways, it is difficult to assign a HC(O)OH emission rate solely to wetland emission, however it would appear that wetland emission is likely to be an important contributing factor. A recent estimation of HC(O)OH wetland emission approximates an emission factor of $2.5 \times 10^{-4} \text{ mg}_{[\text{HCOOH}]} \cdot \text{m}^{-2} \cdot \text{h}^{-1}$ [5], whereas work from this study estimates an emission factor over 29 times greater than this. This highlights the need for additional research on HC(O)OH release from wetlands, of which constrained ground-based flux studies are best suited to complement this work. The additional flux measurement in September (case study B804) identified a change in this region from a surface source to a surface sink. The average temperature and relative humidity between the August and September flux concentration measurements were very similar suggesting these components are unlikely to be the driving factors behind the observed change in this region from a source to a sink.

Delineation of wetland soils in this region may also provide further insight into the emission process. The lack of surface measurements within the wetland region, however, make it difficult to hypothesise a single cause for this change, however, based on the available information, we hypothesise that soil moisture content is likely an important factor governing this process change. From this work, it is clear that further studies are required to fully assess wetlands as a source of HC(O)OH and to investigate its impact on the regional atmospheric budget, particularly in the Arctic region. This work would suggest seasonal, ground-based flux chamber studies in this wetland region are required to better constrain and interpret gaseous HC(O)OH emission from this source type. However, based on the observed HC(O)OH flux from case study B796b, wetlands may represent a much greater emission source of HC(O)OH in the Arctic summer, than previously thought.

Acknowledgments: This work was funded by the UK NERC, under the auspices of the MAMM project, (grant # NE/I029293/1). The authors would like to acknowledge Alan Knights, University of Bristol, for analysing the HC(O)OH calibration gas mixture using GC-FID analysis. We would also like to thank the FAAM staff for providing core aircraft data and their assistance in fitting the CIMS on-board the aircraft and DFL for coordinating the MAMM airborne campaign.

Author Contributions: The experiments were conceived by John Pyle, Euan Nisbet, Martin Gallagher, Grant Allen, Carl Percival and Dudley Shallcross; designed by Carl Percival, Dudley Shallcross, Keith Bower and Ben Jones, and carried out by Benjamin T Jones, Asan Bacak, Jennifer Muller, Stephane Bauguitte, Sebastian O'Shea, Carl Percival, Dudley Shallcross, Michael Le Breton, and James France. Isotope studies were carried out by Euan Nisbet,

Rebecca Fisher and Dave Lowry. Thomas Bannan's contribution concerns the development and operation of the CIMS instrument, which provided the formic acid data used in the study. All authors participated in the data analysis and interpretation and contributed to the manuscript.

Conflicts of Interest: The authors declare no conflict of interest.

References

1. Dawson, G.A.; Farmer, J.C.; Jarvis, L.M. Formic and acetic acids in the atmosphere of the southwest U.S.A. *Geophys. Res. Lett.* **1980**, *7*, 725–728. [[CrossRef](#)]
2. Keene, W.C.; Galloway, J.N.; Holden, J.D. Measurement of weak organic acidity in precipitation from remote areas of the world. *J. Geophys. Res.* **1983**, *88*, 5122–5130. [[CrossRef](#)]
3. Andreae, M.O.; Talbot, R.W.; Andreae, T.W.; Harriss, R.C. Formic and acetic acid over the central amazon region, Brazil 1. Dry season. *J. Geophys. Res.* **1988**, *93*, 1616–1624. [[CrossRef](#)]
4. Bannan, T.J.; Bacak, A.; Muller, J.B.A.; Murray, A.M.; Jones, B.T.; Le Breton, M.; Leather, K.E.; Ghalaieny, M.; Xiao, P.; Shallcross, D.E.; et al. Importance of direct anthropogenic emissions of HC(O)OH measured by a chemical ionisation mass spectrometer (CIMS) during the Winter ClearfLo Campaign in London, January 2012. *Atmos. Environ.* **2013**, *83*, 301–310. [[CrossRef](#)]
5. Paulot, F.; Wunch, D.; Crounse, J.D.; Toon, J.C.; Millet, B.D.; DeCarlo, P.F.; Vigouroux, C.; Deutscher, N.M.; Abad, G.G.; Notholt, J.; et al. Importance of secondary sources in the atmospheric budgets of formic and acetic acids. *Atmos. Chem. Phys.* **2011**, *11*, 1989–2013. [[CrossRef](#)]
6. Jacob, D.J. Chemistry of OH in remote cloud and its role in the production of HC(O)OH and peroxymonosulphate. *J. Geophys. Res.* **1986**, *91*, 9807–9826. [[CrossRef](#)]
7. Gonzalez, A.G.; Bernath, P.F.; Boone, C.D.; McLeod, S.D.; Manney, G.L.; Toon, G.C. Global distribution of upper tropospheric HC(O)OH from the ACE-FTS. *Atmos. Chem. Phys.* **2009**, *9*, 8039–8047. [[CrossRef](#)]
8. Stavrakou, T.; Müller, J.-F.; Peeters, J.; Razavi, A.; Clarisse, L.; Clerbaux, C.; Coheur, P.F.; Hurtmans, D.; De Mazière, M.; Vigouroux, C.; et al. Satellite evidence for a large source of HC(O)OH from boreal and tropical forests. *Nat. Geosci.* **2011**, *5*, 26–30. [[CrossRef](#)]
9. Le Breton, M.; McGillen, M.R.; Muller, J.B.A.; Bacak, A.; Shallcross, D.E.; Xiao, P.; Huey, L.G.; Tanner, D.J.; Coe, H.; Percival, C.J. Airborne observations of formic acid using a chemical ionisation mass spectrometer. *Atmos. Meas. Tech.* **2012**, *5*, 3029–3039. [[CrossRef](#)]
10. Neeb, P.; Sauer, F.; Horie, O.; Moortgat, G.K. Formation of hydroxymethyl hydroperoxide and formic acid in alkene ozonolysis in the presence of waer vapour. *Atmos. Environ.* **1997**, *31*, 1417–1423. [[CrossRef](#)]
11. Kesselmeier, J.; Bode, K.; Gerlach, C.; Jork, E.-M. Exchange of atmospheric formic and acetic acids with trees and crop plants under controlled chamber and purified air conditions. *Atmos. Environ.* **1998**, *32*, 1765–1775. [[CrossRef](#)]
12. Sanhueza, E.; Andreae, M.O. Emission of formic and acetic acids from tropical savannah soils. *Geophys. Res. Lett.* **1991**, *18*, 1707–1710. [[CrossRef](#)]
13. Kawamura, K.; Ng, L.-L.; Kapan, I.R. Determination of organic acids (C1–C10) in the atmosphere, motor exhausts, and engine oil. *Environ. Sci. Technol.* **1985**, *19*, 1082–1086. [[CrossRef](#)] [[PubMed](#)]
14. Talbot, R.W.; Beecher, K.M.; Hariss, R.C.; Cofer, W.R., III. Atmospheric geochemistry of formic and acetic acids in mid-latitude temperate site. *J. Geophys. Res.* **1998**, *93*, 1638–1652. [[CrossRef](#)]
15. Talbot, R.W.; Andreae, M.O.; Berresheim, H.; Jacob, D.J.; Beecher, K.M. Sources and sinks of formic, acetic, and pyruvic acids over central Amazonia 2. Wet season. *J. Geophys. Res.* **1990**, *95*, 16799–16811. [[CrossRef](#)]
16. Graedel, T.E.; Weschler, C.J. Chemistry within aqueous atmospheric aerosols and raindrops. *Rev. Geophys.* **1981**, *19*, 505–539. [[CrossRef](#)]
17. Jones, B.T.; Muller, J.B.A.; O'Shea, S.; Bacak, A.; Le Breton, M.; Bannan, T.J.; Leather, K.E.; Booth, A.M.; Illingworth, S.; Bower, K.; et al. Airborne measurements of HC(O)OH in the European Arctic: A winter-summer comparison. *Atmos. Environ.* **2014**, *99*, 556–567. [[CrossRef](#)]
18. Grutter, M.; Glatthor, N.; Stiller, G.P.; Fischer, H.; Grabowski, U.; Hopfner, M.; Kellmann, S.; Linden, A.; von Clarmann, T. Global distribution and variability of HC(O)OH as observed by MIPAS-ENVISAT. *J. Geophys. Res.* **2010**, *115*, D10303. [[CrossRef](#)]
19. Sposito, G. *The Chemistry of Soils*; Oxford University Press: Oxford, UK, 1989.

20. Forster, P.; Ramaswamy, V. Changes in atmospheric constituents and in radiative forcing. In *Climate Change 2007: The Physical Science Basis*; Cambridge University Press: Cambridge, UK, 2007; pp. 129–234.
21. Parmentier, F.-J.W.; Christensen, T.R.; Sorensen, L.L.; Rysgaard, S.; McGuire, A.D.; Miller, P.A.; Walker, D.A. The impact of lower sea-ice extent on Arctic greenhouse gas exchange. *Nat. Clim. Chang.* **2013**, *3*, 195–202. [[CrossRef](#)]
22. Leibowitz, S.G. Isolated wetlands and their functions: An ecological perspective. *Soc. Wetl. Sci.* **2003**, *23*, 517–531. [[CrossRef](#)]
23. Oelke, C.; Zhang, T.J.; Serreze, M.C. Modelling evidence for recent warming of the Arctic soil thermal regime. *Geophys. Res. Lett.* **2004**, *31*. [[CrossRef](#)]
24. Mausbach, M.J.; Richardson, J.L. Biogeochemical processes in hydric soil formation. *Curr. Top. Wetl. Biogeochem.* **1994**, *1*, 68–127.
25. Soil Grids. Available online: https://www.soilgrids.org/#/?lon=22.12646484375&lat=68.29987352961231&zoom=9&layer=geonode:taxnwr_b_250m&showInfo=1 (accessed on 14 June 2017).
26. Nowak, J.B.; Neuman, J.A.; Kozai, K.; Huey, L.G.; Tanner, D.J.; Holloway, J.S.; Ryerson, T.B.; Frost, G.J.; McKeen, S.A.; Fehsenfeld, F.C. A chemical ionization mass spectrometry technique for airborne measurements of ammonia. *J. Geophys. Res. Atmos.* **2007**, *112*, D10S02. [[CrossRef](#)]
27. Slusher, D.L.; Huey, L.G.; Tanner, D.J.; Flocke, F.M.; Roberts, J.M. A thermal dissociation-chemical ionization mass spectrometry (td-cims) technique for the simultaneous measurement of peroxyacyl nitrates and dinitrogen pentoxide. *J. Geophys. Res.* **2004**, *109*, D19315. [[CrossRef](#)]
28. O'Shea, S.J.; Bauguitte, S.J.B.; Gallagher, M.W.; Lowry, D.; Percival, C.J. Development of a cavity-enhanced absorption spectrometer for airborne measurements of CH₄ and CO₂. *Atmos. Meas. Tech.* **2013**, *6*, 1095–1109. [[CrossRef](#)]
29. Lewis, A.C.; Evans, M.J.; Hopkins, J.R.; Punjabi, S.; Read, K.A.; Purvis, R.M.; Andrews, S.J.; Moller, S.J.; Carpenter, L.J.; Lee, J.D.; et al. The influence of biomass burning on the global distribution of selected non-methane organic compounds. *Atmos. Chem. Phys.* **2011**, *13*, 851–867. [[CrossRef](#)]
30. Keeling, C.D. The concentration and isotopic abundance of atmospheric carbon dioxide in rural areas. *Geochim. Cosmochim. Acta* **1958**, *13*, 322–334. [[CrossRef](#)]
31. Keeling, C.D. The concentration and isotopic abundances of carbon dioxide in rural and marine air. *Geochim. Cosmochim. Acta* **1961**, *24*, 277–298. [[CrossRef](#)]
32. Gerbig, C.; Schmitgen, S.; Kley, D.; Volz-Thomas, A. An improved fast-response vacuum-UV resonance fluorescence CO instrument. *J. Geophys. Res.* **1999**, *104*, 1699–1704. [[CrossRef](#)]
33. Real, E.; Law, K.S.; Weinzierl, B.; Fiebig, M.; Petzold, A.; Wild, O.; Methven, J.; Arnold, S.; Stohl, A.; Huntrieser, H.; et al. Processes influencing ozone levels in Alaskan forest fire plumes during long range transport over the North Atlantic. *J. Geophys. Res. Atmos.* **2007**, *112*, D10S41. [[CrossRef](#)]
34. O'Shea, S.J.; Allen, G.; Gallagher, M.W.; Bower, K.; Illingworth, S.M.; Muller, J.B.A.; Jones, B.T.; Percival, C.J.; Bauguitte, S.J.-B.; Cain, M.; et al. Methane and carbon dioxide fluxes and their regional scalability for the European Arctic wetlands during the MAMM project in summer 2012. *Atmos. Chem. Phys.* **2014**, *14*, 13159–13174. [[CrossRef](#)]
35. White, W.H.; Anderson, J.A.; Blumenthal, D.L.; Husar, R.B.; Gillani, N.V.; Husar, J.D.; Wilson, W.E. Formation and transport of secondary air-pollutants-ozone and aerosols in St-Louise urban plume. *Science* **1976**, *194*, 187–189. [[CrossRef](#)] [[PubMed](#)]
36. Gallagher, M.W.; Choularton, T.W.; Bower, K.N.; Stromberg, I.M.; Beswick, K.M.; Fowler, D.; Hargreaves, K.J. Measurements of methane fluxes on the landscape scale from a wetland area in north Scotland. *Atmos. Environ.* **1994**, *28*, 2421–2430. [[CrossRef](#)]
37. Choularton, T.W.; Gallagher, M.W.; Bower, K.N.; Fowler, D.; Zahniser, M.; Kaye, A. Trace gas flux measurements at the landscape scale using boundary-layer budgets. *Phil. Trans. R. Soc. A* **1995**, *351*, 357–368. [[CrossRef](#)]
38. Wratt, D.S.; Gimson, N.R.; Brailsford, G.W.; Lassey, K.R.; Bromley, A.M.; Bell, M.J. Estimating regional methane emissions from agriculture using aircraft measurements of concentration profiles. *Atmos. Environ.* **2001**, *35*, 497–508. [[CrossRef](#)]
39. Mays, K.L.; Shepson, P.B.; Stirm, B.H.; Karion, A.; Sweeney, C.; Gurney, K.R. Aircraft-based measurements of the carbon footprint of Indianapolis. *Environ. Sci. Technol.* **2009**, *43*, 7816–7823. [[CrossRef](#)] [[PubMed](#)]

40. Karion, A.; Sweeney, C.; Petron, G.; Frost, G.; Hardesty, R.M.; Kofler, J.; Miller, B.R.; Newberger, T.; Wolter, S.; Banta, R.; et al. Methane emissions estimate from airborne measurements over a western United States natural gas field. *Geophys. Res. Lett.* **2013**, *40*, 1–5. [[CrossRef](#)]
41. Le Breton, M.; Bacak, A.; Muller, J.B.A.; O’Shea, S.J.; Xiao, P.; Ashfold, M.N.R.; Cooke, M.C.; Batt, R.; Shallcross, D.E.; Oram, D.E.; et al. Airborne hydrogen cyanide measurements using a chemical ionisation mass spectrometer for the plume identification of biomass burning forest fires. *Atmos. Chem. Phys.* **2013**, *13*, 9217–9232.
42. Veres, P.; Roberts, J.M.; Warneke, C.; Welsh-Bon, D.; Zahniser, M.; Herndon, S.; Fall, R.; de Gouw, J. Development of negative-ion proton-transfer chemical-ionization mass spectrometry (NI-PT-CIMS) for measurement of gas-phase organic acids in the atmosphere. *Int. J. Mass Spectrom.* **2008**, *274*, 48–55. [[CrossRef](#)]
43. Bridgman, S.D.; Cadillo-Quiroz, H.; Keller, J.K.; Zhuang, G. Methane emissions from wetlands: Biogeochemical, microbial, and modelling perspectives from local to global scales. *Glob. Chang. Biol.* **2013**, *19*, 1325–1346. [[CrossRef](#)] [[PubMed](#)]
44. Fisher, R.E.; Sriskantharajah, S.; Lowry, D.; Lanoiselle, M.; Fowler, C.M.R.; James, R.H.; Hermansen, O.; Lund Myhre, C.; Stohl, A.; Greinert, J.; et al. Arctic methane sources: Isotopic evidence for atmospheric inputs. *Geophys. Res. Lett.* **2011**, *38*, L21803. [[CrossRef](#)]
45. Sriskantharajah, S.; Fisher, R.E.; Lowry, D.; Aalto, T.; Hatakka, J.; Aurela, M.; Laurila, T.; Lohila, A.; Kuitunen, E.; Nisbet, E.G. Stable carbon isotope signatures of methane from a Finnish subarctic wetland. *Tellus B* **2012**, *64*, 18818. [[CrossRef](#)]
46. Papen, H.; Rennenberg, H. Microbial processes involved in emissions of radiatively important trace gases. In Proceedings of the Transactions 14th International Congress of Soil Science, Kyoto, Japan, 12–18 August 1990; Volume II, pp. 232–237.
47. O’Connor, F.M.; Boucher, O.; Gedney, N.; Jones, C.D.; Folberth, G.A.; Coppel, R.; Friedlingstein, P.; Collins, W.J.; Chappellaz, J.; Ridley, J.; et al. Possible role of wetlands, permafrost, and methane hydrates in the methane cycle under future climate change: A review. *Revs. Geophys.* **2010**, *48*, RG4005. [[CrossRef](#)]
48. Corine Land Cover 2006. Available online: <http://www.eea.europa.eu/data-and-maps/data/corine-land-cover-2006-raster> (accessed on 22 June 2017).



© 2017 by the authors. Licensee MDPI, Basel, Switzerland. This article is an open access article distributed under the terms and conditions of the Creative Commons Attribution (CC BY) license (<http://creativecommons.org/licenses/by/4.0/>).